Electron-impact excitation of the $(\ldots 6s5d\,^1D_2)$ to $(\ldots 6s6p\,^1P_1)$ transition in barium

P. V. Johnson, B. Eves, and P. W. Zetner
Department of Physics, University of Manitoba, Winnipeg MB, Canada R3T 2N2

D. Fursa and I. Bray
School of Physical Sciences, Flinders University of South Australia, GPO Box 2100, Adelaide 5001, Australia
(Received 27 May 1998)

We have measured and calculated scattering parameters (differential cross sections and four electron-impact coherence parameters) for electron-impact excitation of the $(\ldots 6s5d\,^1D_2)$ to $(\ldots 6s6p\,^1P_1)$ transition in barium in the low to intermediate impact energy regime (10, 20, and 40 eV). Measurements were carried out by the superelastic scattering technique in which collisional deexcitation from the laser-excited $(\ldots 6s6p\,^1P_1)$ state to the metastable $(\ldots 6s5d\,^1D_2)$ level was detected by electron-energy-loss spectroscopy in a crossed-beam apparatus. Supporting calculations were carried out in the convergent close-coupling scheme. Measured differential cross sections were significantly lower than those measured for $(\ldots 6s6p\,^1P_1)$ excitation out of the ground $(\ldots 6s^2\,^1S_0)$ state and good agreement with theory was found. Measured and calculated coherence parameters show strikingly different behavior from that associated with $^1P_1$ excitations out of the ground state. Agreement between measured and calculated coherence parameters was found to be less satisfactory than in the case of the differential cross sections but was, nevertheless, encouraging considering the weak nature of the transition. [S1050-2947(99)08301-8]

PACS number(s): 34.80.Dp

I. INTRODUCTION

Electron collisions with excited atoms play a prominent role in a variety of partially ionized plasma systems (high-density gas discharges; astrophysical, fusion, and semiconductor-etching plasmas; electron-beam and discharge-pumped lasers; etc.) and the basic physics of such collisions must be understood before successful theoretical models of these systems can be generated. Collisions involving long-lived metastable species are especially interesting because significant populations of these can accumulate in such plasmas. However, the investigation of electron scattering from excited-state atomic targets represents a relatively unexplored frontier. The challenge to the experimentalist lies in producing sufficient excited atom number densities in the scattering apparatus while the theoretical challenge arises from the need to generate accurate excited-state wave functions and include coupling to the many-target states lying energetically close to the initial and final states.

Schemes to generate metastable atoms (particularly rare-gas metastables) in sufficient concentrations to make scattering experiments feasible have been under development for some time. Such metastable sources based on discharge excitation, electron beam excitation, and charge exchange have been reviewed by Trajmar and Nickel [1] and Lin and Anderson [2]. Measurements of integral inelastic and ionization cross sections have been made using sources of this type. However (angular) differential cross-section measurements are extremely rare because selection of electrons scattered into a specific solid angle can reduce the measured scattering signal by four or more orders of magnitude and higher concentrations of excited target species are therefore required.

For some atomic systems (such as alkali-metal or alkaline-earth elements), limitations on excited atom number densities encountered in the sources listed above can be overcome by employing laser pumping. Continuous-wave laser light tuned to the resonance (S to P) wavelength in these atoms has been successfully employed in differential scattering experiments carried out on sodium (Jiang *et al.* [3], Sang *et al.* [4], Sholten *et al.* [5], Hermann and Hertel [6], Hertel and Stoll [7]), chromium (Hanne *et al.* [8]), ytterbium (Li and Zetner [9]), calcium (Law and Teubner [10]) and barium (Li and Zetner [11–13], and Zetner *et al.* [14–16]). These investigations have all been concerned with scattering out of a short-lived, excited P state and, for the most part, have concentrated on the superelastic P to S deexcitation process. The aim has been to measure the dependence of the superelastic scattering signal on laser polarization and incidence direction in order to extract the so-called electron impact coherence parameters (EICP) for the ''time-inverse'' S to P excitation as discussed further below. Apart from the work of Jiang *et al.* [3] in sodium and Li and Zetner [13] and Zetner *et al.* [16] in barium, very little work has been done on inelastic-scattering differential cross-section measurements out of the excited P state.

The present study concerns itself with experimental and theoretical investigation of the $(\ldots 6s5d\,^1D_2)$ to $(\ldots 6s6p\,^1P_1)$ excitation in barium. Level designations are those of Moore [17] in which the dominant $^{2S+1}L_J$ term and the dominant contributing configuration are indicated. The $1s^22s^22p^63s^23p^63d^{10}4s^24p^64d^{10}5s^25p^6$ configuration is abbreviated by an ellipsis. When laser radiation tuned to the ^{138}Ba resonance transition [$(\ldots 6s^2\,^1S_0)$ to $(\ldots 6s6p\,^1P_1)$ at 553.7 nm] interacts with a beam of barium atoms, substantial concentrations of $(\ldots 6s6p\,^1P_1)$ and $(\ldots 6s5d\,^{1,3}D)$ are produced. The metastable D levels are populated by radiative cascade from the $^1P_1$ level. When electrons scatter from this target beam of mixed ground- and excited-state constituents, a variety of processes become accessible to

study. Inelastic processes of the type $(\ldots 6s6p\,^1P_1)$ to X, where X represents some higher-lying level, have recently been reported by Zetner *et al.* [16]. An important aspect of such processes is the coherent nature of the laser-excited $(\ldots 6s6p\,^1P_1)$ state. Coherence in this context refers to the preparation of a quantum mechanically pure $^1P_1$ magnetic sublevel superposition state and its effect on the measurement of the differential cross section (DCS) is discussed by Zetner *et al.* [16]. Processes originating on the metastable D levels (i.e., $^{1,3}D$ to X) are also observable (Zetner *et al.* [18]). In principle, the excited D levels should be partially coherent in nature as a result of their production (by radiative cascade) from a fully coherent $^1P_1$ state.

When the DCS for a particular type of inelastic process is to be measured, the most straightforward method involves the analysis of an electron-energy-loss spectrum in the inelastic region of interest. The objective is to isolate an energy-loss feature corresponding to a particular excitation and convert the intensity of this feature to the associated DCS. This presents a difficult task, however, because the large number of observable processes leads to a highly congested spectrum (under conditions of practical electron energy resolution) and, consequently, rather involved unfolding procedures must be utilized.

The experimental data presented in this work extend our previous investigations (Li and Zetner [12,13]) in which we focus on the $(\ldots 6s5d\,^1D_2)$ to $(\ldots 6s6p\,^1P_1)$ excitation. Isolation of this particular process was accomplished by turning our attention to a related process, namely the $(\ldots 6s6p\,^1P_1)$ to $(\ldots 6s5d\,^1D_2)$ deexcitation, which is well-resolved in the superelastic portion of the energy-loss spectrum. The exact nature of the (''time-inverse'') relationship between the superelastic process we study and the inelastic process we wish to describe will be discussed in the next section. Here we point out that the coherent nature of the laser-excited $^1P_1$ state allows us to probe fine details of the excitation (as characterized by the EICP) in addition to measuring the DCS. To our knowledge, the only previous studies of this type are a set of measurements carried out by Hermann [19] involving electron impact excitation of the laser-prepared Na$(3\,^2P)$ state to the higher-lying $3\,^2D$ level at 5 eV impact energy and scattering angles less than 25°. These measurements remained unpublished until the review by Andersen *et al.* [20], where they were analyzed in terms of the ^2D to ^2P superelastic collision.

The theoretical method employed in the present work for calculation of electron scattering from the $(\ldots 6s5d\,^1D_2)$ level is the convergent close-coupling (CCC) method. This method was successfully applied to the calculation of electron scattering from hydrogen (Bray and Stelbovics [21]), light alkali-metal atoms (Li: Karaganov *et al.* [22]; Na: Bray [23]) and helium (Fursa and Bray [24]). It was generalized to a calculation of electron scattering from alkali-metal earth atoms and results for electron-beryllium scattering have been reported (Fursa and Bray [25]).

Until recently the CCC method has been applied to the calculation of electron scattering from relatively light targets. Calculation of electron scattering from a target as heavy as barium poses a new challenge. Our first results at the single incident electron energy of 20 eV for elastic scattering and excitation from the barium ground state (Fursa and Bray [26]) and for elastic scattering from the $(\ldots 6s6p\,^1P_1)$ state (Trajmar *et al.* [27]) are in good quantitative agreement with experimental data.

This paper is organized as follows. Section II describes the measurement theory required to analyze the superelastic scattering data in terms of EICP and the DCS for the ''time-inverse'' inelastic process, Sec. III gives a discussion of the convergent close-coupling (CCC) theory used to calculate scattering parameters (EICP and DCS) while the experimental approach is outlined in Sec. IV. In Sec. V, a comparison of theory and experiment is made, with discussion of general trends observed in the behavior of the scattering parameters. Concluding remarks will be made in Sec. VI.

II. MEASUREMENT THEORY

When resonant, narrow-band, cw laser light interacts with a beam of barium atoms, experimental conditions can be chosen (Register *et al.* [28]) so that only the $(\ldots 6s6p\,^1P_1)$ level of the ^{138}Ba atom is excited by the laser. This simple excitation scheme (as opposed to the alkali-metal atom case, for example, in which nonzero nuclear spin plays a role) leads to the optical preparation of a quantum mechanically pure state, i.e., a coherent superposition of $^1P_1$ magnetic substates: $|J,\mu\rangle$ (for $J=1$ and $\mu=-1,0,+1$). The nature of this coherent superposition state will change depending on the choice of reference frame used to describe it. For linearly polarized laser light it is useful to define the so-called ''photon frame'' (Hertel and Stoll [7], Zetner *et al.* [29]) in which the quantization axis is chosen to lie along the electric-field vector of the linearly polarized light. In this frame, a pure $|1,0\rangle$ magnetic substate is excited. Likewise, for circularly polarized laser light, the pure substate $|1,+1\rangle$ or $|1,-1\rangle$ is excited (depending on the handedness of the polarization) if we describe the state with respect to a quantization axis pointing antiparallel to the laser beam incidence direction (the ''laser frame,'' Macek and Hertel [30]). These pure $|J,\mu\rangle$ substates can be rotated into any convenient reference frame by standard rotation matrix algebra (Brink and Satchler [31]) to produce a coherent superposition of magnetic basis states referenced to a quantization axis identified in this frame. We can write this state as

$$|JN\rangle = a_{-1}|J,-1\rangle + a_0|J,0\rangle + a_{+1}|J,+1\rangle \qquad (1)$$

with magnetic basis states $|J,\mu\rangle$ in the new reference frame and superposition coefficients a_μ. The superposition coefficients a_μ are then functions of the spherical polar angles θ_ν and ϕ_ν which define the laser beam incidence direction with respect to the new quantization axis (and, in the case of linearly polarized light, an angle Ψ which defines the direction of the polarization plane with respect to the quantization axis).

An important reference frame is the so-called ''collision'' frame in which the quantization axis points along the momentum vector, $\vec{k}$, of the incident electron. The electron scatters with new momentum, $\vec{k}'$, so that $\vec{k}$ and $\vec{k}'$ define the scattering plane. We fix coordinate axes to the collision frame by denoting $\hat{z}$ as a unit vector pointing along the quantization axis and $\hat{x}$ as a unit vector lying in the scattering plane so that $\vec{k}'\cdot\hat{x}$ is positive for scattering to the left. In our

earlier work (Li and Zetner [13]) we defined a spin-averaged ''partial'' differential cross section (PDCS) for excitation of a level with basis states $|J',m\rangle$ out of the coherent $|J,N\rangle$ superposition state by

$$\sigma^{\mathrm{PDCS}}=\tfrac{1}{2}\sum_{\mu_s}\sum_{m_s}\frac{k'}{k}\sum_{m}|\langle J'mm_s\vec{k}'|\hat{T}|JN\mu_s\vec{k}\rangle|^2. \quad (2)$$

Here $\langle J'mm_s\vec{k}'|\hat{T}|JN\mu_s\vec{k}\rangle$ is the collision frame scattering amplitude expressed as a matrix element of the transition operator $\hat{T}$. It gives the amplitude for excitation of the $|J'm\rangle$ substate from the laser-excited $|JN\rangle$ coherent superposition state with incident electron momentum $\vec{k}$ and spin μ_s and scattered electron momentum $\vec{k}'$ and spin m_s. By substituting Eq. (1) into Eq. (2) and defining the (observable) quantities

$$\rho^c_{ij}=\frac{\left\{\sum_m \langle J'm|\hat{T}|Ji\rangle\langle J'm|\hat{T}|Jj\rangle^*\right\}}{\left\{\sum_m\sum_\mu|\langle J'm|\hat{T}|J\mu\rangle|^2\right\}}, \quad (3)$$

where the curly brackets represent an average over incident electron spins and a sum over scattered electron spins, we can write the PDCS for any laser beam geometry (defined by the angles θ_ν,ϕ_ν) and polarization state.

For linearly polarized laser light, the PDCS is a function of laser angles $(\theta_\nu,\phi_\nu,\psi)$ and we are interested in the geometries $(\theta_\nu,\phi_\nu)=(90°,90°)$ and $(\theta_\nu,\phi_\nu)=(90°,45°)$, for which it can be shown that

$$\sigma^{\mathrm{PDCS}}(90°,90°,\psi)=\tfrac{3}{4}\sigma^{\mathrm{DCS}}\begin{pmatrix}1-\cos 2\psi\\ +(1+3\cos 2\psi)\rho^c_{00}\\ -2(1-\cos 2\psi)\rho^c_{-11}\\ +4\sqrt{2}\ \sin 2\psi\ \mathrm{Re}[\rho^c_{01}]\end{pmatrix} \quad (4)$$

and

$$\sigma^{\mathrm{PDCS}}(90°,45°,\psi)=\tfrac{3}{4}\sigma^{\mathrm{DCS}}\begin{pmatrix}1-\cos 2\psi\\ +(1+3\cos 2\psi)\rho^c_{00}\\ +4\sin 2\psi\ \mathrm{Re}[\rho^c_{01}]\end{pmatrix}, \quad (5)$$

where the symbol σ^{DCS} represents the DCS.

For circularly polarized light, the PDCS is a function of the handedness of the polarization and the laser angles (θ_ν,ϕ_ν). For the $(\theta_\nu,\phi_\nu)=(90°,90°)$ geometry, we have

$$\sigma^{\mathrm{PDCS}}_{\pm}(90°,90°)=\tfrac{3}{4}\sigma^{\mathrm{DCS}}(1+\rho^c_{00}-2\rho^c_{-11}\pm 4\sqrt{2}\ \mathrm{Im}[\rho^c_{01}]), \quad (6)$$

where the ''$\pm$'' subscript indicates right-hand $(+)$ or left-hand $(-)$ circularly polarized light.

The scattering intensity I for some collision process involving the $|JN\rangle(^1P_1)$ target state is proportional to the PDCS, i.e., for linearly polarized laser light,

$$I(\theta_\nu,\phi_\nu,\psi)=\kappa\sigma^{\mathrm{PDCS}}(\theta_\nu,\phi_\nu,\psi), \quad (7a)$$

or, for circularly polarized laser light,

$$I_\pm(\theta_\nu,\phi_\nu)=\kappa\sigma^{\mathrm{PDCS}}_\pm(\theta_\nu,\phi_\nu), \quad (7b)$$

where the proportionality constant κ contains factors such as detection solid angle, detection efficiency, incident electron flux, and the number of laser-excited P level atoms within the interaction volume.

From Eqs. (4)–(6) it can be seen that the scattering intensity depends on laser beam incidence angles θ_ν and ϕ_ν, laser beam polarization state, and scattering parameters: σ^{DCS}, ρ^c_{00}, ρ^c_{-11}, $\mathrm{Re}[\rho^c_{01}]$, and $\mathrm{Im}[\rho^c_{01}]$. The parameters ρ^c_{ij} have an interesting physical significance first discussed by Macek and Hertel [30]. They can be interpreted as density-matrix elements for an excited P level produced in a collision process related by time reversal to the measured process. For example, if the superelastic scattering signal associated with collisional deexcitation of the coherent $^1P_1$ state to the ground $^1S_0$ state is measured, then the density-matrix elements ρ^c_{ij} refer to the time inverse $^1S_0$ to (coherent) $^1P_1$ inelastic process. In our present studies we measure the superelastic scattering signal arising from the (coherent) $^1P_1$ to $^1D_2$ deexcitation to determine matrix elements, ρ^c_{ij}, for the $^1D_2$ to $^1P_1$ (coherent) excitation. A key point here is that, while superelastic scattering from the coherent $^1P_1$ state will generally result in an anisotropic distribution of population among the $^1D_2$ magnetic sublevels (as determined by the superelastic scattering amplitudes $\langle J'm|\hat{T}|JN\rangle$), the inelastic process described by matrix elements ρ^c_{ij} involves excitation out of a $^1D_2$ level in which all magnetic sublevels are equally populated. This is made manifest by the summation over m which appears in Eq. (2) as a consequence of the fact that the $^1D_2$ magnetic sublevels remain unresolved in the superelastic scattering experiment.

Blum [32] has discussed symmetry conditions which restrict the number of real parameters required to completely specify the density matrix for a collisionally excited P state. The requirements of hermiticity and reflection invariance in the scattering plane restrict the required number of independent, real parameters to four (for the normalization $\Sigma_i\rho^c_{ii}=1$) when the initial level is isotropically populated. Thus, with the inclusion of the DCS, five real scattering parameters can completely specify the (isotropic) $^1D_2$ to $^1P_1$ excitation with unpolarized electrons, namely σ^{DCS}, ρ^c_{00}, ρ^c_{-11}, $\mathrm{Re}[\rho^c_{01}]$, and $\mathrm{Im}[\rho^c_{01}]$. The partial differential cross sections defined in Eqs. (4)–(6) can be measured to extract each of these scattering parameters. However, it is more convenient to measure appropriate combinations of these quantities which define the EICP discussed in the review of Andersen *et al.* [20]. Our experimental method can provide direct measurements of the DCS, the Stokes parameters P_1, P_2, and P_3, and the λ parameter by making use of the following combinations of partial differential cross sections:

$$\frac{\sigma^{\mathrm{PDCS}}(90°,90°,0°)-\sigma^{\mathrm{PDCS}}(90°,90°,90°)}{\sigma^{\mathrm{PDCS}}(90°,90°,0°)+\sigma^{\mathrm{PDCS}}(90°,90°,90°)}=P_1, \quad (8a)$$

$$\frac{\sigma^{\mathrm{PDCS}}(90°,90°,45°)-\sigma^{\mathrm{PDCS}}(90°,90°,135°)}{\sigma^{\mathrm{PDCS}}(90°,90°,45°)+\sigma^{\mathrm{PDCS}}(90°,90°,135°)}=P_2, \quad (8b)$$

$$\frac{\sigma_+^{\mathrm{PDCS}}(90°,90°)-\sigma_-^{\mathrm{PDCS}}(90°,90°)}{\sigma_+^{\mathrm{PDCS}}(90°,90°)+\sigma_-^{\mathrm{PDCS}}(90°,90°)}=P_3, \tag{8c}$$

$$\frac{\sigma^{\mathrm{PDCS}}(90°,45°,0°)}{\sigma^{\mathrm{PDCS}}(90°,45°,0°)+2\sigma^{\mathrm{PDCS}}(90°,45°,90°)}=\lambda, \tag{8d}$$

and

$$\tfrac{1}{3}[\sigma^{\mathrm{PDCS}}(90°,45°,0°)+2\sigma^{\mathrm{PDCS}}(90°,45°,90°)]=\sigma^{\mathrm{DCS}}. \tag{8e}$$

Since the scattering parameters defined in Eqs. (8a)–(8e) refer to the time-inverse process, we must make use of the appropriate collision frame with which to describe this process. In this work, we measure the superelastic process to understand the inelastic process. The collision frame quantization axis appropriate to the time-inverse inelastic process of interest lies antiparallel to the superelastically scattered electron momentum vector. The laser angles θ_ν, ϕ_ν, and ψ are measured with respect to this axis.

The EICP given by Eqs. (8a)–(8d) describe excitation out of the isotropic $^1D_2$ level to the $^1P_1$ state. These parameters would be identical to those measured in an electron-photon coincidence experiment carried out on a target beam of ^{138}Ba $^1D_2$ metastable atoms in which the inelastically scattered electron, having excited the $^1P_1$ state, is detected in time correlation with the $^1P_1$ to $^1S_0$ fluorescence photon. Determination of the DCS by Eq. (8e) requires a normalization procedure which is briefly described below. For details, we refer the reader to Li and Zetner [13].

III. COLLISION THEORY

We refer to Fursa and Bray [25] for the details of calculation of electron scattering from alkali-metal earth atoms. Here we give a brief overview of the method and details specific to e-Ba scattering. The CCC method is formulated in a nonrelativistic LS coupling framework. The total wave function (projectile and target electrons) is expanded in a basis of barium target states. The close-coupling equations for the T matrix (coupled Lippman-Schwinger equations) are then formulated and solved in momentum space.

For barium target states we adopt a model of two valence electrons above an inert Hartree-Fock core. Standard configuration-interaction (CI) expansion has been used to obtain barium atom energy levels and wave functions. One-electron orbitals used in the CI expansion have been calculated by diagonalization of the Ba^+ ion Hamiltonian in a Sturmian (Laguerre) basis. The resulting barium target states are square-integrable. Negative energy states (relative to the Ba^+ ground state) represent an approximation to the barium discrete spectrum states, while positive energy states provide square-integrable discretization of the barium continuum, allowing, therefore, coupling to the ionization channels.

In order to account for polarizability of the inert core, we have added phenomenological one-electron and two-electron polarization potentials. The cutoff parameters of the one-electron polarization potential have been chosen to fit the energies of the low-lying states of the Ba^+ ion. The set of two electron configurations in the CI expansion has been constructed from one-electron orbitals with orbital angular momentum $l=0$, 1, 2, and 3. One of the electrons in the configuration set has been restricted to occupy the Ba^+ $6s$, $7s$, $6p$, $7p$, and $5d$ orbitals only, while the number of orbitals (within given l) for the other electron has been increased to achieve convergence in the description of the low-lying discrete states of the barium atom. We have found that such a choice of configurations is sufficient to account for a major part of the electron-electron correlations.

The accuracy of the Ba wave functions involved in the present study can be estimated by comparing experimental and calculated energy levels and oscillator strengths. For the $(\ldots 6s^2\,{}^1S)$, $(\ldots 6s6p\,{}^1P_1)$, and $(\ldots 6s5d\,{}^1D_2)$ levels, theoretical (experimental) ionization energies are 5.237 (5.211), 2.973 (2.972), and 3.978 (3.978) eV, respectively, where the experimental values are from Moore [17]. The calculated oscillator strength for the $(\ldots 6s^2\,{}^1S)$ to $(\ldots 6s6p\,{}^1P_1)$ transition is 1.64 a.u., in agreement with the experimental value of 1.64 a.u. (Hulpke *et al.* [33]). For the $(\ldots 6s5d\,{}^1D_2)$ to $(\ldots 6s6p\,{}^1P_1)$ transition, the calculated value of 0.0035 a.u. is in accord with the experimental estimate for the oscillator strength being less than 0.0034 a.u. (Bernhardt *et al.* [34]). The modified form of the dipole length operator has been used to calculate oscillator strengths (Laughlin and Victor [35], Hameed *et al.* [36]). The very small value of the $(\ldots 6s5d\,{}^1D_2)$ to $(\ldots 6s6p\,{}^1P_1)$ oscillator strength makes it extremely sensitive to the details of the calculation with the error in the relatively small energy difference between the two states being one of the major factors contributing to the sensitivity. We therefore have varied the cutoff parameter of the two-electron polarization potential to achieve the best fit to the $(\ldots 6s6p\,{}^1P_1)$ and $(\ldots 6s5d\,{}^1D_2)$ ionization energies.

Barium is a heavy atom for which relativistic effects are expected to be important. The spin-orbit term is the major relativistic correction and leads to singlet-triplet mixing of the barium levels. This mixing for the levels involved in the present study, $(\ldots 6s6p\,{}^1P_1)$-$(\ldots 6s6p\,{}^3P_1)$ and $(\ldots 6s5d\,{}^1D_2)$-$(\ldots 6s5d\,{}^3D_2)$, was found to be small (Trefitz [37], Bauschlicher, Jr. *et al.* [38]). Our scattering calculations indicate that, at the incident electron energies of 10, 20, and 40 eV, the cross section for excitation of the triplet states is significantly smaller than the cross section for excitation of the corresponding singlet states. We therefore believe that the present nonrelativistic theoretical model is adequate. A similar conclusion was reached in the experimental (Li and Zetner [11]) and theoretical (Clark *et al.* [39], Srivastava *et al.* [40]) studies of $(\ldots 6s6p\,{}^1P_1)$ level excitation from the barium ground state. Finally, we would like to refer to the work of Zeman *et al.* [41], who tested the nonrelativistic approximation for e-Cs scattering in the framework of the distorted-wave method. They found that relativistic effects were important for spin-resolved scattering but not important for the spin-averaged quantities. As the cross sections and electron-photon coincidence parameters studied in this work involve averaging over spin and magnetic sublevels, we believe relativistic effects to be relatively unimportant.

The present calculations have been performed in two models: a 55-state close-coupling calculation [CC(55)] and a 115-state convergent close-coupling calculation [CCC(115)]. The 55-state close-coupling calculations in-

volve only discrete spectrum states. It comprises five ^1S, six $^1P^o$, seven $^1D^e$, five $^1F^o$, three ^3S, six $^3P^o$, five $^3D^e$, five $^3F^o$, one $^1P^o$, three $^1D^o$, one $^1F^e$, three $^3P^e$, three $^3D^o$, and two $^3F^e$, states. In order to estimate the effect of the coupling to the barium atom ionization continuum, we performed the 115-state close-coupling calculations which included a large number of positive energy states and comprise $14\,^1S$, $17\,^1P^o$, $19\,^1D^e$, $19\,^1F^o$, $7\,^3S$, $9\,^3P^o$, $9\,^3D^e$, $9\,^3F^o$, and two each of $^{1,3}P^e$, $^{1,3}D^o$, and $^{1,3}F^e$ states.

IV. EXPERIMENTAL METHOD

The apparatus consists of an electron spectrometer in which the electron source and scattered electron detector both employ single-hemisphere energy selection optics. Measurements were carried out with a system energy resolution of about 170 meV, sufficient to separate the $^1P_1$ to $^1D_2$ superelastic energy-loss feature (at -0.83 eV) from the tail of the elastic feature. The angular resolution of the spectrometer is estimated to be less than 5°. Magnetic-field compensation (to less than 25 mG) is accomplished by a single layer of 0.050 in. μ-metal shielding which is periodically degaussed.

The electron spectrometer is configured in such a way that the scattered electron detector is held fixed while the electron gun is rotatable. This establishes the most convenient geometry for measuring scattering parameters associated with a ''time-reversed'' process. The ''time-reversed'' collision frame quantization axis lies antiparallel to the scattered electron momentum vector, hence along the fixed detector axis pointing away from the detector. Laser polar angles θ_ν and ϕ_ν (as well as laser beam polarization angle ψ) are then referenced to this fixed axis.

The metal vapor beam source consists of a tubular, 304 stainless-steel crucible wrapped with resistive, coaxial heating wire. It is heated to a typical operating temperature of 760 °C and produces a beam collimation of 10:1 with typical number densities of the order of 7×10^{10} cm^{-3} at the interaction region. During a measurement, background gas pressure in the chamber was typically less than 1×10^{-6} torr.

Schematic diagrams of the apparatus are presented in Fig. 1. Figure 1(a) shows an experimental configuration in which the laser beam strikes the scattering plane perpendicularly, $(\theta_\nu,\phi_\nu)=(90°,90°)$, while Fig. 1(b) shows the $(\theta_\nu,\phi_\nu)=(90°,45°)$ geometry in which the laser beam strikes the scattering plane at 45° and the detector axis at 90°. In each case, the atom beam is directed in such a way that it is transversely illuminated by the laser beam. The purpose of transverse illumination is to limit the Doppler width of the absorption line, thereby allowing selection of the zero-nuclear-spin ^{138}Ba isotope for optical excitation. Requirements on atom beam collimation, laser beam intensity, and residual fields necessary for isolation of the ^{138}Ba isotope are discussed in detail by Register *et al.* [28].

Selection of the polarization state of the laser beam at the interaction region was accomplished by a phase retardation plate (P in Fig. 1) in tandem with a Glan-Taylor polarizing prism (GT in Fig. 1).

Use of the perpendicular geometry, $(\theta_\nu,\phi_\nu)=(90°,90°)$, with linearly polarized laser light allows the determination of the Stokes parameters P_1 and P_2 through

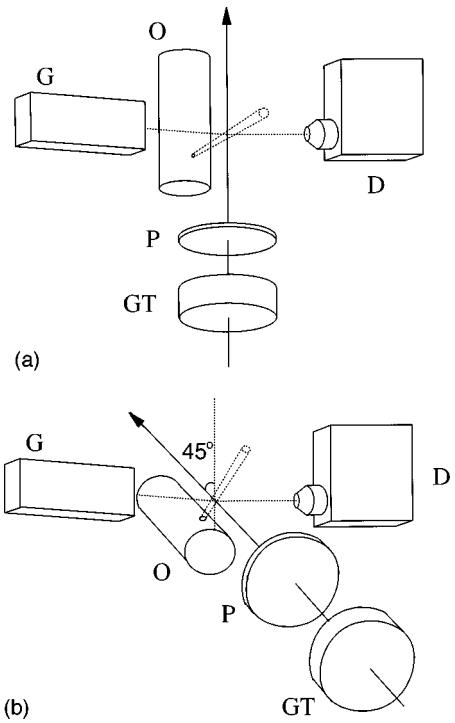

FIG. 1. A schematic diagram of the apparatus is shown for experimental configurations involving the two laser geometries: (a) $(\theta_\nu,\phi_\nu)=(90°,90°)$ and (b) $(\theta_\nu,\phi_\nu)=(90°,45°)$. The electron source ($G$), electron detector ($D$), atom beam source ($O$), Glan-Taylor polarizing prism (GT), and phase-retardation plate (P) are shown.

Eqs. (8a) and (8b). With circularly polarized laser light, we can measure the P_3 Stokes parameter by Eq. (8c). Note that the Stokes parameters $P_1, P_2,$ and P_3 are determined entirely by *ratios* of PDCS measurements which can be obtained, under stable experimental conditions, simply from ratios of scattering intensities.

The $(\theta_\nu,\phi_\nu)=(90°,45°)$ geometry, in conjunction with linearly polarized laser light, is useful for the measurement of the DCS and the λ parameter as shown in Eqs. (8d) and (8e). The λ parameter, as in the case of the Stokes parameters, is again determined by the appropriate ratio of scattering intensities.

Measurements of $P_1, P_2, P_3,$ and λ were carried out by rotating P, the retardation plate, into the desired orientation with a motor drive and accumulating signal counts in a scaler. After some preset interval, a timing signal was used to rotate P into the new orientation required for the determination of a particular scattering parameter. Signal was again accumulated in a (different) scaler so that the desired ratio of scattering intensities could be found. The measurement proceeded in an automated fashion and included a detection channel in which background signal was collected by activating a shutter to block the laser beam.

The DCS determination requires the weighted average of *normalized* PDCS values given in Eq. (8e). The paper of Li and Zetner [13] describes in detail a reliable normalization scheme in which the Ba(. . . $6s5d\,^1D_2$) to (. . . $6s6p\,^1P_1$) excitation can be calibrated to known values of the (. . . $6s^2\,^1S_0$) to (. . . $6s6p\,^1P_1$) excitation previously measured by Jensen *et al.* [42] and Wang *et al.* [43]. Essentially,

the procedure involves a measurement of the relative scattering intensities, combined according to Eq. (8e), for the $(\ldots 6s6p\,^1P_1)$ to $(\ldots 6s5d\,^1D_2)$ and $(\ldots 6s6p\,^1P_1)$ to $(\ldots 6s^2\,^1S_0)$ superelastic transitions with an application of the principle of detailed balance to give the inelastic DCS. The measurement of the DCS proceeded in a fashion similar to that employed in the determination of λ and the Stokes parameters, except that additional detection channels were required for the accumulation of $^1P_1$ to $^1S_0$ superelastic signal for each polarization state. This involved an automated adjustment of electron spectrometer voltages to give the required energy loss and impact energy.

V. RESULTS AND DISCUSSION

Figures 2–6 show the results of the present work. Measured parameters are compared with the 55-state close-coupling [CC(55)] and convergent close-coupling [CCC(115)] calculations. At incident energy $E_0=20$ eV, calculations of the DCS and the λ parameter carried out in the unitarized distorted wave approximation (UDWA) are also shown (Clark and Csanak [44]; see also Clark *et al.* [39]). Measurements of the DCS (Fig. 2) reveal forward-peaking behavior as expected for a dipole-allowed excitation. This forward peaking becomes more pronounced with increasing impact energy. Table I gives a listing of the measured relative DCS (with respect to the $^1S_0$ to $^1P_1$ DCS as well as the normalized results corresponding to the values plotted in Fig. 2. From the table it is apparent that the $^1D_2 \rightarrow {}^1P_1$ DCS is significantly smaller than the $^1S_0$ to $^1P_1$ DCS. The small relative DCS is consistent with the small branching fraction for $^1P_1$ to $^1D_2$ radiative decay relative to the $^1P_1$ to $^1S_0$ radiative transition (Bizzarri and Huber [45]). Close-coupling calculations reveal the same forward-peaking trend as the measurements and exhibit good quantitative agreement at small scattering angles. Agreement between CC(55) and CCC(115) calculations is good, with the former DCS being larger than the latter. This is consistent with the effect of coupling to the ionization channels.

Figure 3 shows the behavior of the λ parameter at incident energies $E_0=10$, 20, and 40 eV. This parameter gives the PDCS for excitation of the $^1P_1$ $(m=0)$ sublevel relative to the DCS for excitation of the $^1P_1$ level (all sublevels). Agreement between measurement and CCC(115) theory is quite good. In Figs. 4, 5, and 6 our results for the P_1, P_2, and P_3 Stokes parameters are presented. The measured parameters and those calculated in the close-coupling schemes are in qualitative agreement. Measured parameters are listed in Table II.

The parameters λ, P_1, P_2, and P_3 represent our raw measurements. Better insight into the collision dynamics can be obtained, however, by converting to the natural parameters $\{L_{\rm perp},\gamma,P^+_{\rm lin},h\}$ of Andersen *et al.* [20]. These parameters are straightforwardly related to the measured parameters and convey physically meaningful information about the angular part of the excited *p*-state charge cloud. The parameters $P^+_{\rm lin}$ and γ give the anisotropy and alignment angle, respectively, of the component of the *p*-state charge cloud which exhibits positive reflection symmetry with respect to the scattering plane. $P^+_{\rm lin}$ measures the relative difference between ''length'' and ''width'' (i.e., maximum density $|\Psi|^2_{\rm max}$ and minimum density $|\Psi|^2_{\rm min}$, respectively) of the excited charge cloud. This parameter takes on a value of 1 when the width

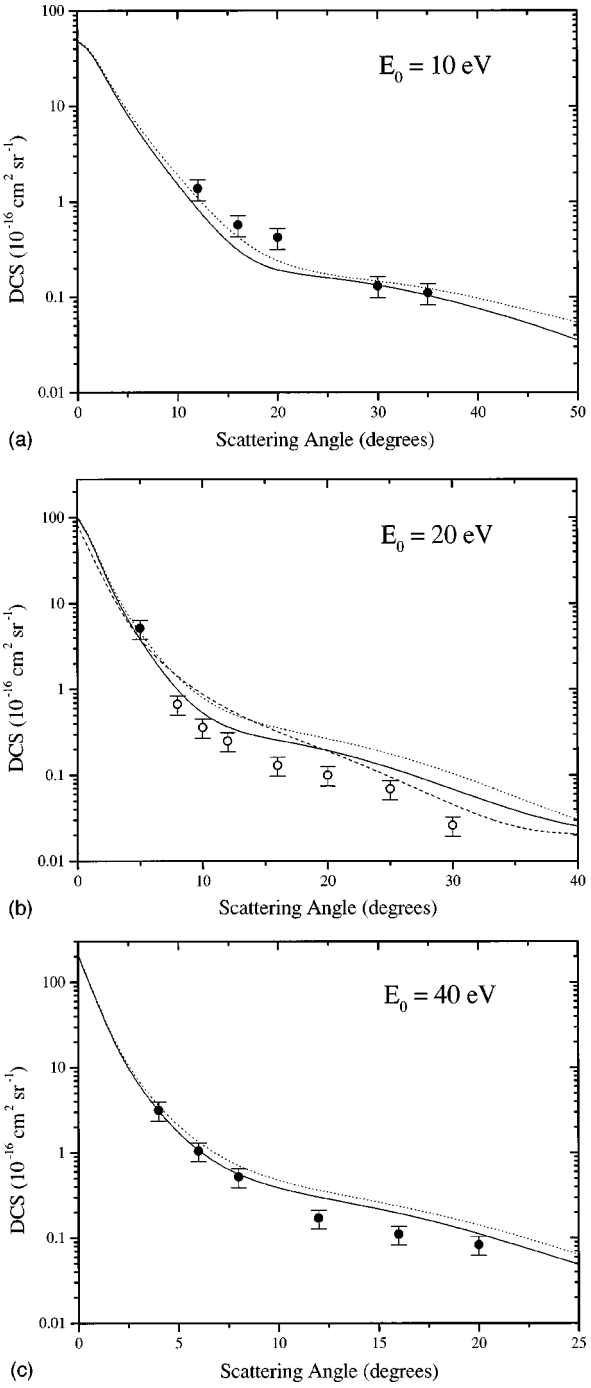

FIG. 2. Measured and calculated differential cross sections for the $^1D_2$ to $^1P_1$ excitation in Ba for impact energies: (a) $E_0=10$ eV, (b) $E_0=20$ eV, and (c) $E_0=40$ eV. The results of convergent close-coupling calculations [CCC(115)] and 55-state close-coupling calculations [CC(55)] are represented by the solid curves and the dotted curves, respectively. Present measurements are shown as solid circles with error bars. The measurements of Li and Zetner [13] are presented as open circles with error bars. Results of a unitarized distorted-wave calculation carried out at 20 eV impact energy (Clark and Csanak [44]) are shown by the dashed curve.

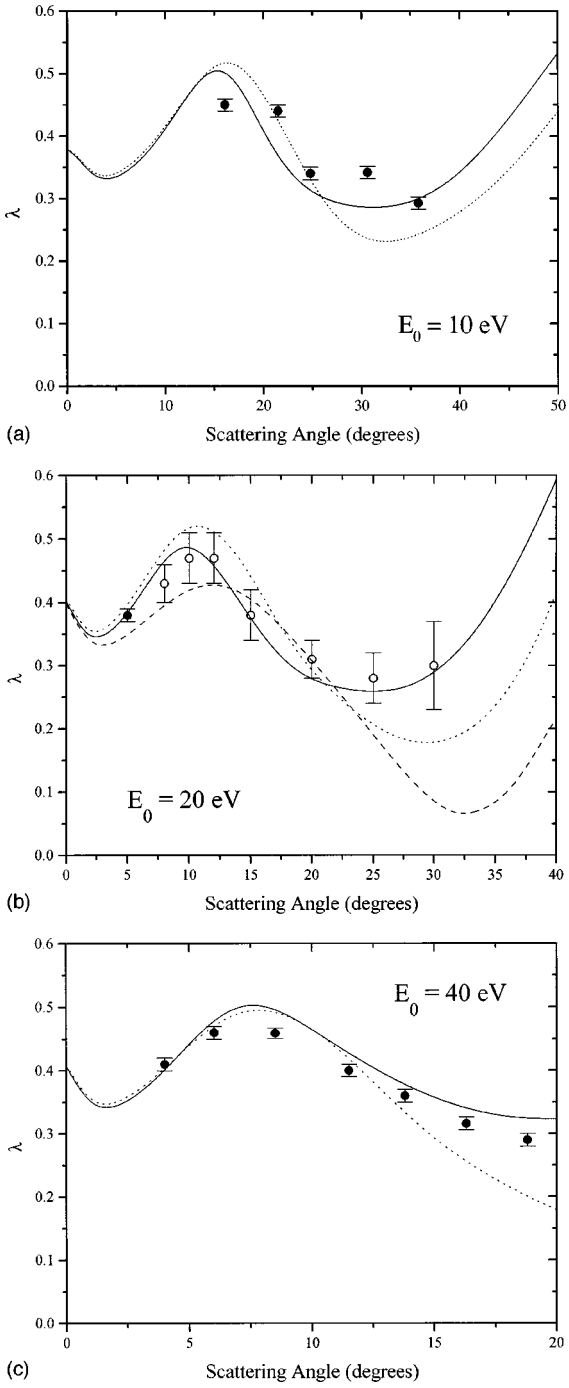

FIG. 3. Measured and calculated λ parameters for the $^1D_2$ to $^1P_1$ excitation in Ba for impact energies: (a) $E_0=10$ eV, (b) $E_0=20$ eV, and (c) $E_0=40$ eV. The results of convergent close-coupling calculations [CCC(115)] and 55-state close-coupling calculations [CC(55)] are represented by the solid curves and the dotted curves, respectively. Present measurements are shown as solid circles with error bars. The measurements of Li and Zetner [13] are presented as open circles with error bars. Results of a unitarized distorted-wave calculation carried out at 20 eV impact energy (Clark and Csanak [44]) are shown by the dashed curve.

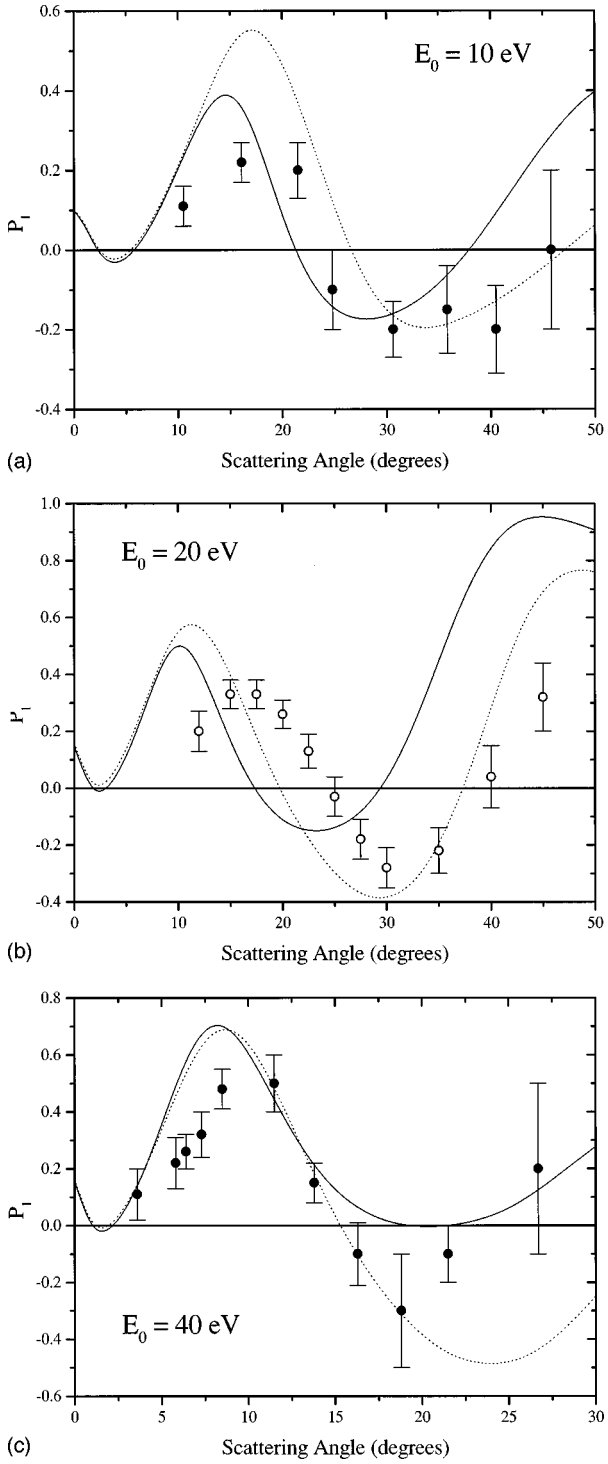

FIG. 4. Measured and calculated values of the P_1 Stokes parameter for the $^1D_2$ to $^1P_1$ excitation in Ba for impact energies: (a) $E_0=10$ eV, (b) $E_0=20$ eV, and (c) $E_0=40$ eV. The results of convergent close-coupling calculations [CCC(115)] and 55-state close-coupling calculations [CC(55)] are represented by the solid curves and the dotted curves, respectively. Present measurements are shown as solid circles with error bars. The measurements of Li and Zetner [12] are presented as open circles with error bars.

goes to zero and a value of zero when the length equals the width. The alignment angle γ gives the direction of maximum charge cloud density with respect to the collision frame quantization axis. The height parameter h gives the relative excitation cross section for the negative reflection symmetry component of the charge cloud. The h parameter is related to the λ parameter in that the former gives the relative cross section for excitation of a p orbital aligned along an axis perpendicular to the scattering plane (the ''natural frame''

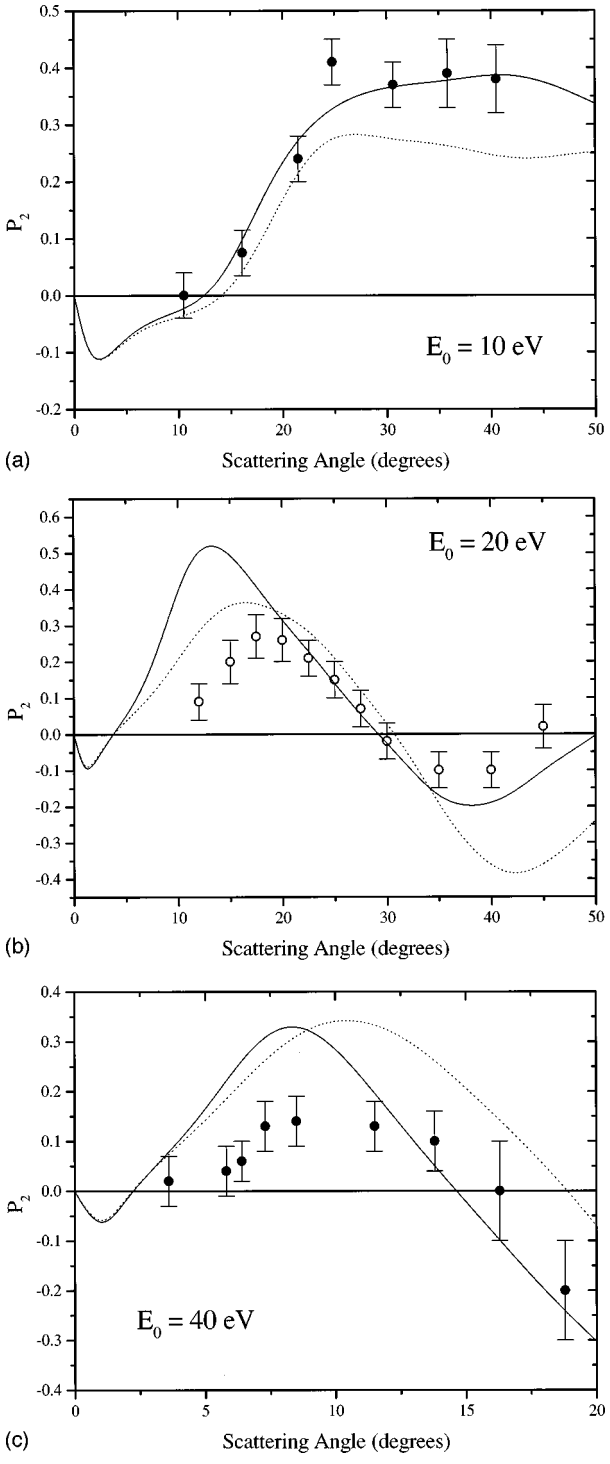

FIG. 5. Measured and calculated values of the P_2 Stokes parameter for the $^1D_2$ to $^1P_1$ excitation in Ba for impact energies: (a) $E_0=10$ eV, (b) $E_0=20$ eV, and (c) $E_0=40$ eV. The results of convergent close-coupling calculations [CCC(115)] and 55-state close-coupling calculations [CC(55)] are represented by the solid curves and the dotted curves, respectively. Present measurements are shown as solid circles with error bars. The measurements of Li and Zetner [12] are presented as open circles with error bars.

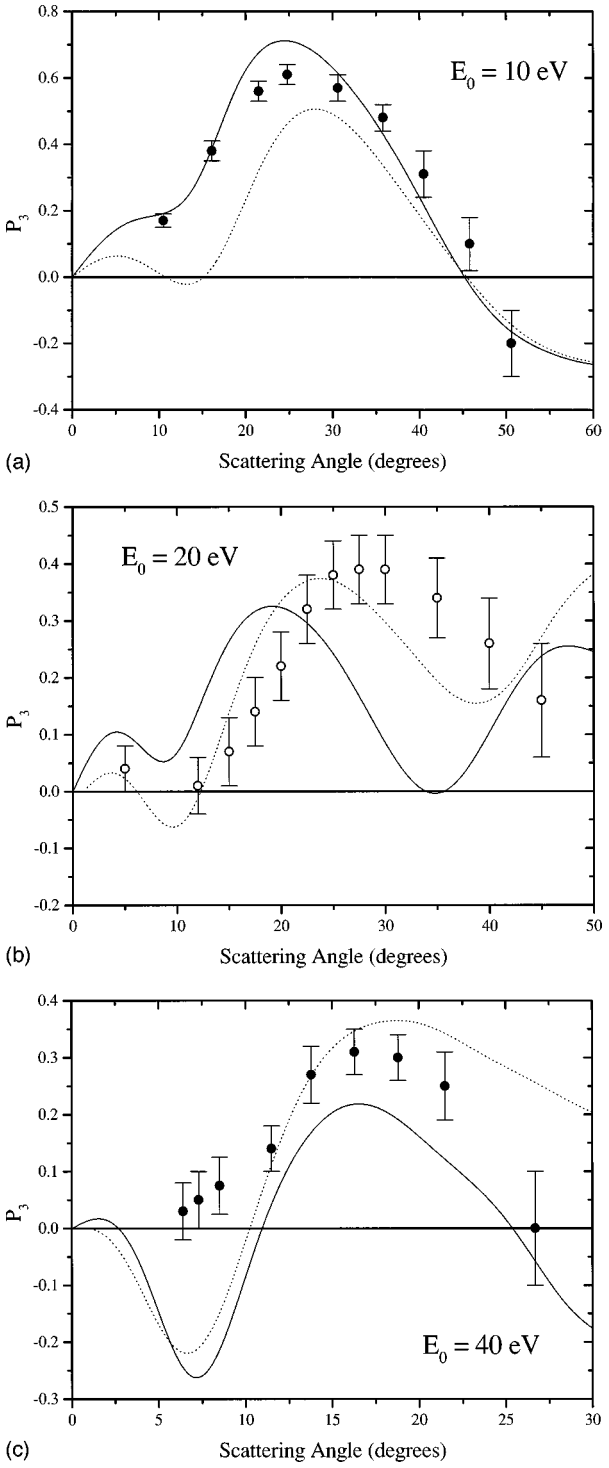

FIG. 6. Measured and calculated values of the P_3 Stokes parameter for the $^1D_2$ to $^1P_1$ excitation in Ba for impact energies: (a) $E_0=10$ eV, (b) $E_0=20$ eV, and (c) $E_0=40$ eV. The results of convergent close-coupling calculations [CCC(115)] and 55-state close-coupling calculations [CC(55)] are represented by the solid curves and the dotted curves, respectively. Present measurements are shown as solid circles with error bars. The measurements of Li and Zetner [12] are presented as open circles with error bars.

quantization axis), while the latter gives the relative excitation cross section for excitation of a p orbital aligned along the collision frame quantization axis. The L_{perp} parameter gives the expectation value of the collisionally transferred orbital angular momentum (measured with respect to the natural frame quantization axis).

Relationships between the measured parameters $\{P_1,P_2,P_3,\lambda\}$ and the natural parameters $\{L_{\text{perp}},\gamma,P_{\text{lin}}^{+},h\}$

TABLE I. Measured differential cross sections.

θ (deg)	10 eV	20 eV[a]	40 eV
	Relative differential cross sections (10^{-2})		
4			0.83(0.01)
5		1.50(0.03)†	
6			0.72(0.01)
8		0.54(0.04)	0.86(0.01)
10		0.58(0.05)	1.50(0.04)
12	1.57(0.03)	0.83(0.08)	4.00(0.08)
16	1.46(0.04)	1.10(0.10)	5.80(0.20)
20	2.50(0.07)	3.60(0.30)	
25		5.20(0.60)	
30	5.30(0.10)	3.30(0.60)	
35	10.0(0.20)		
	Absolute differential cross sections (10^{-16} cm^2 sr^{-1})		
4			3.15(0.79)
5		5.13(1.28)†	
6			1.04(0.26)
8		0.67(0.17)	0.52(0.13)
10		0.36(0.09)	
12	1.37(0.34)	0.25(0.06)	0.17(0.04)
16	0.57(0.14)	0.13(0.03)	0.11(0.03)
20	0.42(0.11)	0.10(0.03)	0.08(0.02)
25		0.07(0.02)	
30	0.13(0.03)	0.03(0.01)	
35	0.11(0.03)		

[a]Tabulated data for $E_0=20$ eV is from Li and Zetner [13] with the exception of the measurement identified by the dagger symbol (†).

TABLE II. Measured coherence parameters.

θ (deg)	P_1	P_2	P_3	λ
		$E_0=10$ eV		
10.5	0.11(0.05)	0.00(0.04)	0.17(0.02)	
16.1	0.22(0.05)	0.075(0.04)	0.38(0.03)	0.45(0.01)
21.5	0.20(0.07)	0.24(0.04)	0.56(0.03)	0.44(0.01)
24.8	−0.10(0.10)	0.41(0.04)	0.61(0.03)	0.34(0.01)
30.6	−0.20(0.07)	0.37(0.04)	0.57(0.04)	0.34(0.01)
35.8	−0.15(0.11)	0.39(0.06)	0.48(0.04)	0.29(0.01)
40.5	−0.20(0.11)	0.38(0.06)	0.31(0.07)	
45.8	0.00(0.20)		0.10(0.08)	
50.6	0.20(0.20)		−0.20(0.10)	
		$E_0=20$ eV[a]		
5			0.04(0.04)	0.38(0.01)†
8				0.43(0.03)
10				0.47(0.04)
12	0.20(0.07)	0.09(0.05)	0.01(0.05)	0.47(0.04)
15	0.33(0.05)	0.20(0.06)	0.07(0.06)	0.38(0.04)
17.5	0.33(0.05)	0.27(0.06)	0.14(0.06)	
20	0.26(0.05)	0.26(0.06)	0.22(0.06)	0.31(0.03)
22.5	0.13(0.06)	0.21(0.05)	0.32(0.06)	
25	−0.03(0.07)	0.15(0.05)	0.38(0.06)	0.28(0.04)
27.5	−0.18(0.07)	0.07(0.05)	0.39(0.06)	
30	−0.28(0.07)	−0.02(0.05)	0.39(0.06)	0.30(0.07)
35	−0.22(0.08)	−0.10(0.05)	0.34(0.07)	
40	0.04(0.11)	−0.10(0.05)	0.26(0.08)	
45	0.32(0.12)	0.02(0.06)	0.16(0.10)	
		$E_0=40$ eV		
3.6	0.11(0.09)	0.02(0.05)		
4.0				0.41(0.01)
5.8	0.22(0.09)	0.04(0.05)		
6.0				0.46(0.01)
6.4	0.26(0.06)	0.06(0.04)	0.03(0.05)	
7.3	0.32(0.08)	0.13(0.05)	0.05(0.05)	
8.5	0.48(0.07)	0.14(0.05)	0.08(0.05)	0.46(0.01)
11.5	0.50(0.10)	0.13(0.05)	0.14(0.04)	0.40(0.01)
13.8	0.15(0.07)	0.10(0.06)	0.27(0.05)	0.36(0.01)
16.3	−0.10(0.11)	0.00(0.10)	0.31(0.04)	0.32(0.01)
18.8	−0.30(0.20)	−0.20(0.10)	0.30(0.04)	0.29(0.01)
21.5	−0.10(0.10)		0.25(0.06)	
26.7	0.20(0.30)		0.00(0.10)	

[a]Tabulated data for $E_0=20$ eV are from Li and Zetner [12,13] with the exception of the measurement identified by the dagger symbol (†).

are given by (see Andersen *et al.* [20])

$$L_{\text{perp}}=\frac{2\lambda P_3}{1+P_1}, \tag{9a}$$

$$P_{\text{lin}}^{+}=(P_1^2+P_2^2)^{1/2}, \tag{9b}$$

$$e^{2i\gamma}=\frac{P_1+iP_2}{(P_1^2+P_2^2)^{1/2}}, \tag{9c}$$

$$1-h=\frac{2\lambda}{1+P_1}. \tag{9d}$$

In their discussion of an excited P state of mixed reflection symmetry, Andersen *et al.* [20] also introduce the parameter L_{perp}^{+} which gives the angular momentum expectation value for the positive reflection symmetry component of the charge cloud. This parameter is directly related to the measured Stokes parameter P_3 by the simple relation $L_{\text{perp}}^{+}=-P_3$ and its behavior can be easily ascertained from Fig. 6. The L_{perp}^{+} and L_{perp} parameters are related by $L_{\text{perp}}=L_{\text{perp}}^{+}(1-h)$ so that the angular momentum expectation value of the excited charge cloud is always diminished when the excitation probability of the negative reflection symmetry component is non-negligible. Natural parameters obtained by employing Eqs. (9a)–(9d) with the measured parameters are tabulated in Table III and plotted in Figs. 7–10 along with appropriate close-coupling calculations.

Figure 7 shows the measured angular behavior of L_{perp} to be well-described by the calculations at 10 eV impact energy while less satisfactory agreement is exhibited at 20 and 40 eV impact energies. It is worth comparing the observed behavior of L_{perp} for the $^1D_2$ to $^1P_1$ excitation to that previously observed in the Ba $^1S_0$ to $^1P_1$ excitation (Li and Zetner [11]), for which it was demonstrated that $h=0$ and, hence, $L_{\text{perp}}=L_{\text{perp}}^{+}$. In the case of $^1S_0$ to $^1P_1$ excitation,

TABLE III. Natural coherence parameters.

θ (deg)	L_{perp}	γ (deg)	P^{+}_{lin}	h	P^{+}
		$E_0=10$ eV			
10.5		0(10.4)	0.11(0.05)		0.20(0.03)
16.1	−0.28(0.03)	9.4(5.1)	0.23(0.05)	0.26(0.03)	0.45(0.04)
21.5	−0.41(0.03)	25.1(5.5)	0.31(0.05)	0.27(0.04)	0.64(0.04)
24.8	−0.46(0.06)	51.9(6.6)	0.42(0.05)	0.24(0.07)	0.74(0.04)
30.6	−0.49(0.06)	59.2(4.4)	0.42(0.05)	0.15(0.05)	0.71(0.04)
35.8	−0.33(0.05)	55.5(7.2)	0.42(0.07)	0.31(0.08)	0.64(0.05)
40.5		58.9(6.8)	0.43(0.07)		0.53(0.07)
		$E_0=20$ eV[a]			
12	−0.008(0.04)	12.1(7.0)	0.22(0.07)	0.22(0.08)	0.22(0.07)
15	−0.04(0.03)	15.6(4.3)	0.39(0.05)	0.43(0.06)	0.39(0.05)
17.5	−0.07(0.03)	19.6(3.8)	0.43(0.05)		0.45(0.05)
20	−0.11(0.03)	22.5(4.3)	0.37(0.05)	0.51(0.05)	0.43(0.06)
22.5	−0.17(0.04)	29.1(6.7)	0.25(0.05)		0.40(0.06)
25	0.22(0.05)	50.7(13.0)†	0.15(0.05)	0.42(0.09)	0.41(0.06)
27.5	−0.28(0.09)	79.4(7.9)†	0.19(0.07)		0.44(0.06)
30	−0.33(0.10)	−88.0(5.1)†	0.28(0.07)	0.17(0.21)	0.48(0.06)
35		−77.8(6.7)†	0.24(0.08)		0.42(0.07)
40		−34.1(27.6)	0.11(0.06)		0.28(0.08)
45		1.8(5.4)	0.32(0.12)		0.36(0.12)
		$E_0=40$ eV			
3.6		5.2(13.3)	0.11(0.09)	0.32(0.06)	
4.0					
5.8		5.2(6.6)	0.22(0.09)	0.23(0.06)	
6.0	−0.008(0.05)				
6.4	−0.02(0.04)	6.5(4.4)	0.27(0.06)		0.27(0.06)
7.3	−0.03(0.03)	11.1(4.6)	0.35(0.08)		0.35(0.08)
8.5	−0.05(0.03)	8.1(3.0)	0.50(0.07)	0.38(0.03)	0.51(0.07)
11.5	−0.07(0.02)	7.3(3.0)	0.52(0.10)	0.47(0.04)	0.54(0.09)
13.8	−0.17(0.03)	16.8(10.1)	0.18(0.07)	0.37(0.04)	0.32(0.06)
16.3	−0.22(0.04)	−90.0(28.6)	0.10(0.11)	0.30(0.09)	0.33(0.05)
18.8	−0.25(0.08)	−73.2(11.0)	0.36(0.18)	0.17(0.24)	0.47(0.14)
21.5	−0.15(0.04)				

[a]Tabulated data for $E_0=20$ eV are from Li and Zetner [12,13]. Data points identified by the dagger symbol (†) are taken from Li and Zetner [12] but corrected for a 90° error in their published values.

studies over a similar kinematic regime ($E_0=20$, 37, and 50 eV) show L_{perp} to take on positive values for small angle scattering ($\theta \lesssim 40°$). A rather broad peak is defined over this region where L_{perp} approaches the maximum value of $+1$ and returns to zero at some scattering angle which depends on impact energy. The condition $L_{perp}=0$ at zero scattering angle is enforced by angular momentum conservation. The $^1S_0$ to $^1P_1$ behavior of L_{perp} in Ba is qualitatively in agreement with the ''generic'' features of S to P excitations discussed by Lin *et al.* [46]. However, for excitation of the $^1P_1$ state from the isotropic $^1D_2$ initial level, as examined in the present work, measurements at impact energy $E_0=10$ eV show an ''inverted'' behavior in which a broad dip is defined with the minimum value of L_{perp} lying near -0.5. Measured results are in close agreement with the CCC(115) calculations. Measured results at higher impact energies point to the same trend as at 10 eV, but close-coupling calculations show an oscillatory behavior in L_{perp} for 20 and 40 eV impact energies with significant positive values attained at 40 eV in the small scattering angle region.

On the basis of the measured results, one is tempted to suggest a propensity rule which links the behavior of L_{perp} to the sign of the change in orbital angular momentum (ΔL) taking place in the collision. For S to P transitions ($\Delta L=+1$), the generic features of L_{perp} behavior have been mentioned above. For the present case of a D to P transition ($\Delta L=-1$), observations indicate similar generic features in the magnitude of L_{perp} but the sign is opposite. A reference to such propensity rules has been made by Andersen *et al.* [20] in their analysis of the Na($3d \rightarrow 3p$) superelastic scattering measurements presented by Hermann [19], but it was pointed out that the utility of such rules for the description of low-energy electron impact is questionable. Considerations of propensity rules and semiclassical models for the behavior of

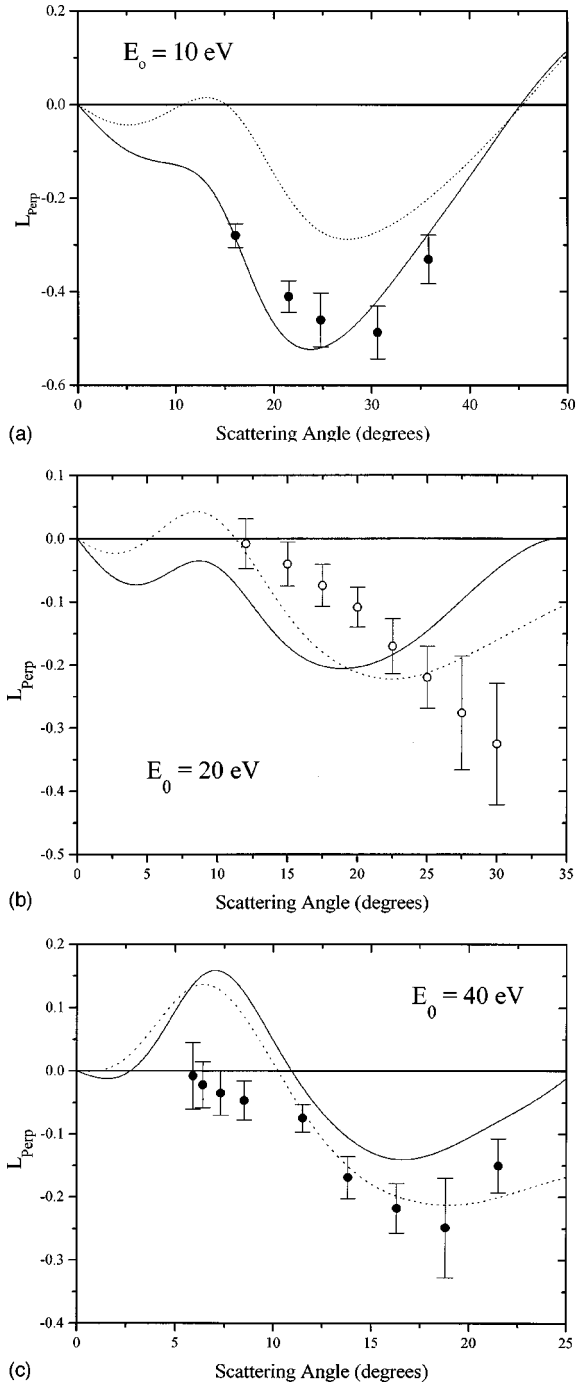

FIG. 7. The L_{perp} parameter for the $^1D_2$ to $^1P_1$ excitation in Ba for impact energies: (a) $E_0=10$ eV, (b) $E_0=20$ eV, and (c) $E_0=40$ eV. The results of convergent close-coupling calculations [CCC(115)] and 55-state close-coupling calculations [CC(55)] are represented by the solid curves and the dotted curves, respectively. Results derived from the present measurements [according to Eq. (9a)] are shown as solid circles with error bars. Results from the measurements of Li and Zetner [12,13] are presented as open circles with error bars.

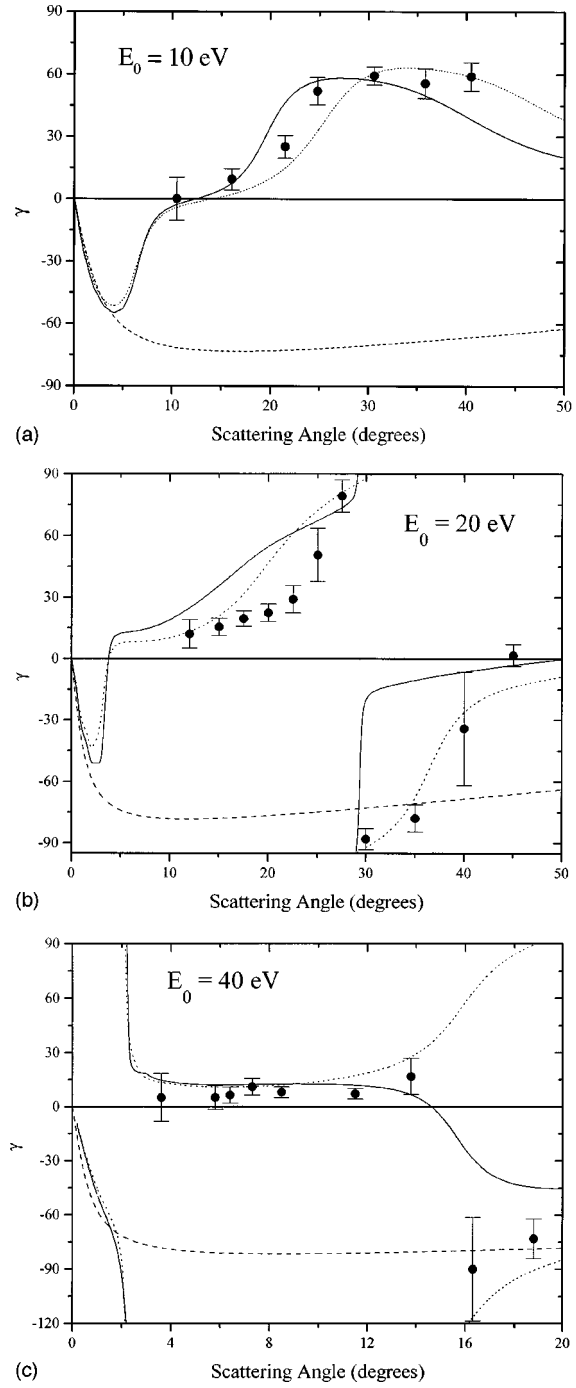

FIG. 8. The alignment angle γ (degrees) for the $^1D_2$ to $^1P_1$ excitation in Ba for impact energies: (a) $E_0=10$ eV, (b) $E_0=20$ eV, and (c) $E_0=40$ eV. The results of convergent close-coupling calculations [CCC(115)] and 55-state close-coupling calculations [CC(55)] are represented by the solid curves and the dotted curves, respectively. Results derived from the present measurements [according to Eq. (9c)] are shown as solid circles with error bars. Results from the measurements of Li and Zetner [12] are presented as open circles with error bars. A calculation in the first Born approximation is represented by the dashed curve.

L_{perp} are discussed in more detail by Lin *et al.* [46], Madison *et al.* [47], Kohmoto and Fano [48], and Hermann and Hertel [49].

Measurements and calculations of the alignment angle are presented in Fig. 8. Good quantitative agreement between measured results and CCC(115) theory is shown at 10 and 40 eV impact energies (for scattering angles smaller than 16° in the 40 eV case). Interestingly, however, the measured data points are in closer agreement with the CC(55) results for the higher impact energies (20 and 40 eV). As in the case of *S* to *P* excitation, the alignment angle can be well described in the

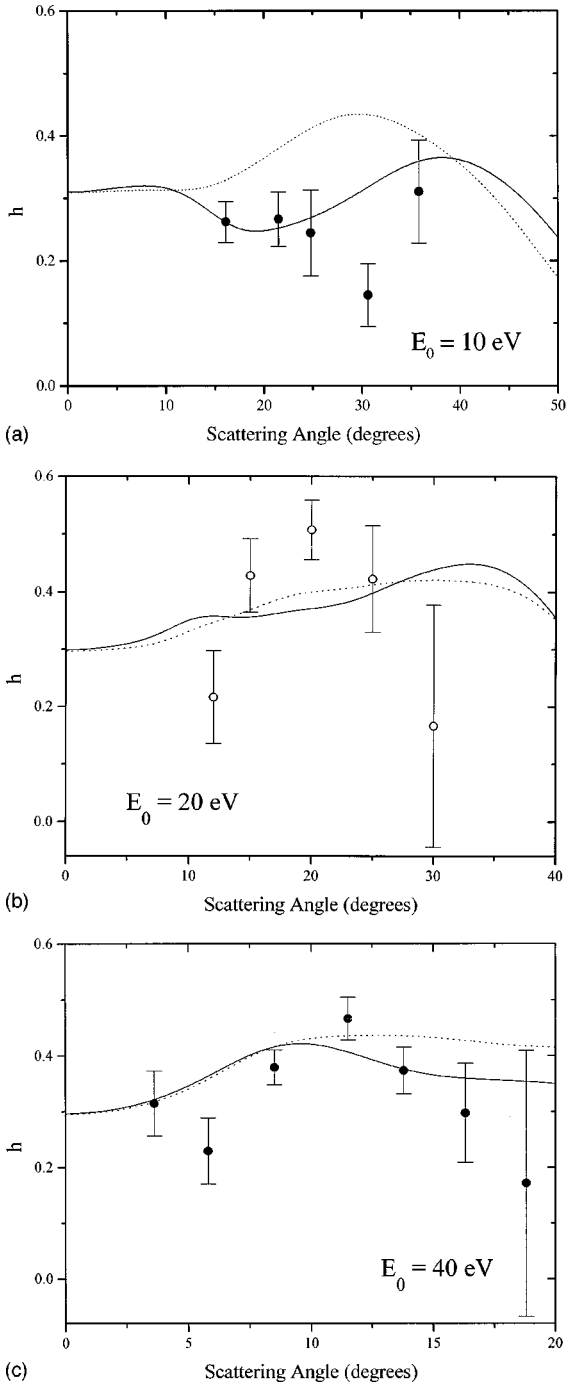

FIG. 9. The height parameter h for the $^1D_2$ to $^1P_1$ excitation in Ba for impact energies: (a) $E_0=10$ eV, (b) $E_0=20$ eV, and (c) $E_0=40$ eV. The results of convergent close-coupling calculations [CCC(115)] and 55-state close-coupling calculations [CC(55)] are represented by the solid curves and the dotted curves, respectively. Results derived from the present measurements [according to Eq. (9d)] are shown as solid circles with error bars. Results from the measurements of Li and Zetner [12,13] are presented as open circles with error bars.

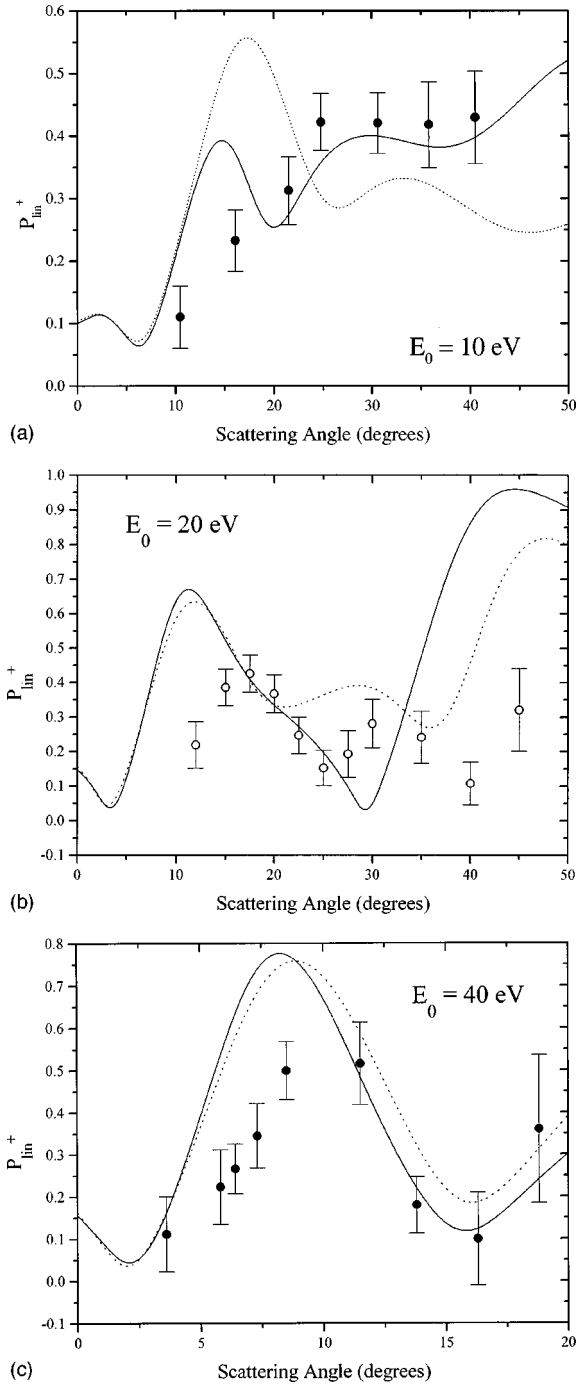

FIG. 10. The anisotropy parameter $P_{\rm lin}^+$ for the $^1D_2$ to $^1P_1$ excitation in Ba for impact energies: (a) $E_0=10$ eV, (b) $E_0=20$ eV, and (c) $E_0=40$ eV. The results of convergent close-coupling calculations [CCC(115)] and 55-state close-coupling calculations [CC(55)] are represented by the solid curves and the dotted curves, respectively. Results derived from the present measurements [according to Eq. (9b)] are shown as solid circles with error bars. Results from the measurements of Li and Zetner [12] are presented as open circles with error bars.

first Born approximation (FBA) for small scattering angles. The reader can consult Andersen *et al.* [20] for examples of this in the case of electron impact excitation of S to P transitions in H, He, and Na. A comparison between measured γ parameters and those calculated in the FBA for the Ba $^1S_0$ to $^1P_1$ excitation was presented by Zetner [50]. The FBA requires the excited P-state charge cloud to exhibit symmetry with respect to the momentum transfer vector and, hence, the alignment angle in the FBA is given by the angular deviation of the momentum transfer vector from the incident electron momentum vector. In contrast to the $^1S_0$ to $^1P_1$ case, the calculated behavior of the $^1D_2$ to $^1P_1$ alignment angle pa-

rameter shows rapid divergence from the FBA at very small scattering angles.

We note that the rapid variation in γ predicted for small scattering angles ($<10°$) is not directly verified by measurement. Small-angle measurements of $^1P_1$ to $^1D_2$ superelastic signal were difficult to make in our apparatus because of a large elastic background. Furthermore, there are inherent limitations to the measurement of low-angle scattering parameters which arise because of the finite angular resolution of the apparatus and the resultant detection of scattering from an interaction volume of finite size. The influence of the finite volume effect on DCS measurements and on EICP measurements has been analyzed by Brinkmann and Trajmar [51] and Zetner *et al.* [29], respectively.

Figure 9 shows calculated and experimentally derived values of the height parameter, *h*, which gives the relative excitation cross section for the negative reflection symmetry component of the charge cloud. The *h* parameter has a special significance in the case of $^1S_0$ to $^1P_1$ excitations in that it signals the presence of spin dependence in the collision interaction. In the absence of spin-dependent forces, the excitation can be described purely in an LS-coupling scheme with the resultant conservation of reflection symmetry of the orbital part of the $^1P_1$ wave function through the scattering plane. Since an initial target $^1S_0$ state has positive reflection symmetry, the final $^1P_1$ state (in the LS-coupling picture) must also have positive reflection symmetry requiring *h* to remain zero. The more complicated $^1D_2$ to $^1P_1$ excitation involves an *initial* target $^1D_2$ level of mixed reflection symmetry. Even in the absence of spin-dependent forces, the negative reflection symmetry component of the $^1P_1$ state can be populated by symmetry-conserving excitations from the negative reflection symmetry components of the $^1D_2$ level. Hence, in the present case, *h* does not give any information about spin effects in the collision.

The charge-cloud anisotropy, $P^+_{\rm lin}$, is provided in Fig. 10. It can be seen from the figure that close-coupling theory has difficulty reproducing the observed behavior of this parameter at all impact energies studied, even in a qualitative sense. On the other hand, the calculations do rather well in describing the alignment angle (Fig. 8). This disparity in predictive power for γ and $P^+_{\rm lin}$ has been observed previously by Martus *et al.* [52] and Zetner *et al.* [15] in their comparison of noble-gas (*S* to *P*) and Ba($^1S_0$ to $^1P_1$) measurements, respectively, to first-order perturbative theories.

Figure 11 gives the behavior of the P^+ parameter which defines the ''degree of polarization'' among the excited *P* states of positive reflection symmetry. It is related to the measured parameters by

$$P^+ = (P_1^2 + P_2^2 + P_3^2)^{1/2} \tag{10}$$

and takes on values lying between the limits of 0 and 1. Although this parameter is not independent of the set of EICP $\{L_{\rm perp}, \gamma, P^+_{\rm lin}, h\}$ described above, it does offer a direct measure of the coherence properties of the collision. In collisional excitation with unpolarized electrons (and spin-insensitive detection), for example, spin-averaged scattering parameters are determined. Incoherence is thus introduced into the description of the collision through the summation over squared amplitudes associated with the two possible

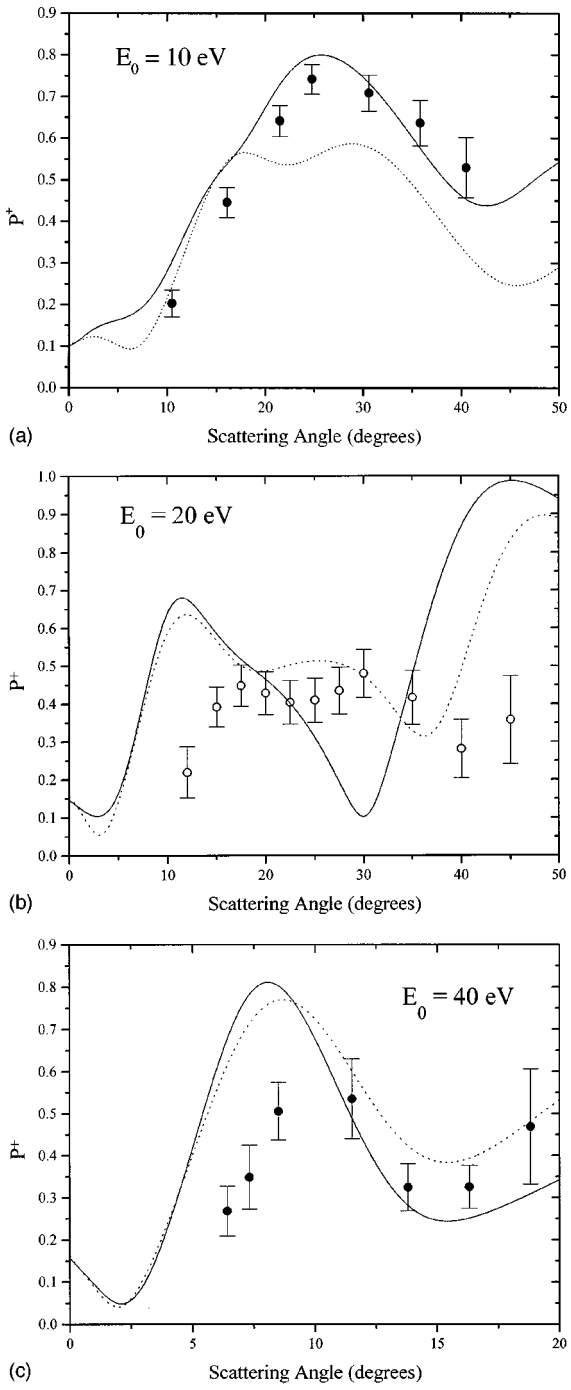

FIG. 11. The polarization parameter P^+ for the $^1D_2$ to $^1P_1$ excitation in Ba for impact energies: (a) $E_0 = 10$ eV, (b) $E_0 = 20$ eV, and (c) $E_0 = 40$ eV. The results of convergent close-coupling calculations [CCC(115)] and 55-state close-coupling calculations [CC(55)] are represented by the solid curves and the dotted curves, respectively. Results derived from the present measurements [according to Eq. (10)] are shown as solid circles with error bars. Results from the measurements of Li and Zetner [12] are presented as open circles with error bars.

electron-spin orientations [the summations over m_s and μ_s in Eq. (2)]. In the case of $^1S_0$ to $^1P_1$ excitations in purely LS-coupled systems (He or Ba, for example), electron spins play an indistinguishable role in the collision with the result that the excitation is fully coherent ($P^+ = 1$). For other *S* to *P* excitations, loss of coherence may occur through exchange

processes (the ^2S to ^2P transitions in H and Na, for example) or spin-flip processes (S to P excitations in the heavy rare gases), in which case P^+ is, generally, less than 1 and provides a useful probe of these spin-dependent effects. For the $^1D_2$ to $^1P_1$ transition under consideration in the present work, an additional source of incoherence arises because of the experimentally unresolved magnetic sublevels in the initial $^1D_2$ level. Assuming conservation of reflection symmetry during the collision, the two positive reflection symmetry components of the $^1P_1$ state can each be excited from three, experimentally unresolved, positive reflection symmetry states in the initial $^1D_2$ level. In principle, one would expect a substantially reduced degree of polarization because of this incoherent contribution to the excitation [made manifest by the summation over m in Eq. (2)]. However, Fig. 11 shows that P^+ can attain surprisingly large values. In the 10 eV impact energy case, for example, peak values close to 0.8 are measured near 25° scattering angle [in agreement with CCC(115) results]. The observation of a relatively high degree of coherence for the $^1D_2$ to $^1P_1$ transition does not have direct significance in terms of exchange or spin-flip processes (as in the case of S to P transitions) but suggests that certain amplitudes must dominate the excitation in this kinematic regime. Figure 11 also shows that, at the higher impact energies, large values of P^+ are predicted by close-coupling theory, but these results are not borne but by the measurements.

Some general comments can be made regarding the behavior of the coherence parameters discussed above in the limit of zero scattering angle. We can demonstrate that the calculated results are consistent with the notion that electron impact excitation becomes equivalent to optical excitation in the zero-momentum-transfer limit. For forward scattering, angular momentum conservation dictates that only $\Delta m=0$ transitions can occur. Hence, only the transitions $^1D_2(m)$ to $^1P_1(m)$ are excited where $m=0,\pm 1$ is the collision frame magnetic sublevel quantum number. If we apply optical selection rules to a $^1D_2$ to $^1P_1$ transition where $\Delta m=0$ (i.e., the case of π-polarized light), we find that the relative excitation probabilities of the $^1P_1$ $(m=0)$ and $^1P_1$ $(m=\pm 1)$ substates are $\frac{4}{10}$ and $\frac{3}{10}$, respectively. Alternatively, in terms of a basis set of $^1P_1$ substates represented by p orbitals aligned along the (x,y,z) collision frame axes (y is perpendicular to the scattering plane), we can express the relative optical excitation probabilities as $(\frac{3}{10}, \frac{3}{10}, \frac{4}{10})$ for the respective p orbitals (p_x,p_y,p_z). Since the λ and h parameters are relative excitation cross sections for the components of the $^1P_1$ state represented by p_z and p_y orbitals, respectively, we immediately find limiting values in forward scattering of $\lambda=\frac{4}{10}$ and $h=\frac{3}{10}$, based on optical selection rules. From Figs. 3 and 9 we can see that close-coupling theory (and the UDWA scheme in the 20 eV case) predicts, to a good approximation, this limiting behavior, especially at the higher impact energies of 20 and 40 eV.

The application of optical selection rules can also give limiting behavior of the alignment angle, γ, and anisotropy parameter, $P^+_{\rm lin}$. Since the optical excitation probabilities for the p_x and p_z orbitals are $\frac{3}{10}$ and $\frac{4}{10}$, respectively, we can see that the major axis of the charge cloud is aligned along the z axis. Hence γ goes to zero in forward scattering in the zero-momentum-transfer limit. The condition $\gamma=0$ implies $P_2=0$, which further implies $P^+_{\rm lin}=P_1$ and then, by Eq. (9d), a limiting value of $P^+_{\rm lin}=\frac{1}{7}$. This limit is demonstrated by the close-coupling results shown in Fig. 10. Note that the condition $L_{\rm perp}=0$ in forward scattering is purely a result of angular momentum conservation without any reference to optical selection rules. By comparison, $^1S_0$ to $^1P_1$ excitations in LS-coupled systems give limiting values of coherence parameters in forward scattering determined solely by the conservation of angular momentum. Specifically, $\lambda=1$, which implies $\gamma=0$, $P^+_{\rm lin}=P_1=1$, and $P_2=0$. In addition, $L_{\rm perp}=0$.

With regard to the behavior of the γ parameter for $^1D_2$ to $^1P_1$ excitation, the suggestion was made by Li and Zetner [13] that the limiting value in forward scattering might be 90° as opposed to 0°. This was based on a comparison of their measured values (at 20 eV impact energy) with a calculation in the FBA. Limiting values of $\gamma=0°$ and 90° in forward scattering both satisfy the symmetry requirement of the charge cloud about the momentum transfer direction in the FBA and measured low-angle values of γ were observed to be consistent with calculations in the FBA carried out for the limiting case of $\gamma=90°$. These authors admit that their measurements could not rule out the possibility of alignment angle behavior which diverges rapidly from FBA predictions in the near-forward-scattering regime. Such a rapid divergence is borne out by the close-coupling calculations presented here which, in agreement with predictions based on optical selection rules, give the limiting value of $\gamma=0°$ in forward scattering.

VI. CONCLUSIONS

We have presented a set of scattering parameters (the differential cross sections and four electron impact coherence parameters) for the $(\ldots 6s5d\,^1D_2)$ to $(\ldots 6s6p\,^1P_1)$ excitation in Ba. When the magnetic sublevel structure of the initial $^1D_2$ level is unresolved (i.e., when this level is isotropically and incoherently populated), these five parameters represent a complete description of the collision process. Measurements were made at impact energies of 10, 20, and 40 eV with supporting calculations carried out in the convergent close-coupling scheme. This work represents a significant extension of previous studies (predominantly of S to P excitations) to the regime of excited-state to excited-state transitions.

Measured differential cross sections for this transition are significantly smaller than those measured for $(\ldots 6s6p\,^1P_1)$ excitation from the ground state and are in good agreement with theory. The small values of the differential cross sections are consistent with the small oscillator strength of this transition. The measured coherence parameters show strikingly different behavior from that previously observed for $^1P_1$ excitations out of the ground state ($^1S_0$). In some cases good agreement with theory is obtained (especially for the λ parameter at all impact energies and for all parameters at 10 eV impact energy) but, in general, calculation of these parameters is, at present, somewhat problematic. The behavior of the coherence parameters for the limiting case of forward scattering is consistent with optical selection rules for $\Delta m=0$ radiative transitions.

A few comments should be made on the accuracy of the

present close-coupling calculations. According to Figs. 2–11, the CCC(115) model is generally in better agreement with experiment than the CC(55) model. On some occasions the CC(55) model is in better agreement with experiment. While this is somewhat disappointing, it should be noted that the $(\ldots 6s5d\,^1D_2)$ to $(\ldots 6s6p\,^1P_1)$ transition is weak, which is indicated by the very small optical oscillator strength. Our scattering calculations indicate that many other transitions have significantly larger excitation cross sections. The $(\ldots 6s5d\,^1D_2)$ excitation ICS is only the twelfth largest ICS at 40 eV, tenth at 20 eV, and seventh at 10 eV [CCC(115) data]. As for any weak transition, we expect our results for the $(\ldots 6s5d\,^1D_2)$ to $(\ldots 6s6p\,^1P_1)$ transition to be more accurate for the ICS than for the DCS, which in turn should be more accurate than the EICP. The achieved level of agreement between the close-coupling calculations and experiment is therefore rather encouraging, and is likely to improve for stronger transitions having $(\ldots 6s5d\,^1D_2)$ as the initial state.

ACKNOWLEDGMENTS

Financial support by the Natural Sciences and Engineering Research Council of Canada, as well as the University of Manitoba, is gratefully acknowledged by P.V.J., B.E., and P.W.Z. These authors also wish to thank S. Trajmar and I. Kanik at the Jet Propulsion Laboratory, Pasadena, California, for a continuing equipment loan. Support by the Australian Research Council and the Flinders University of South Australia is acknowledged by D. Fursa and I. Bray, who also wish to express their indebtedness to the South Australia Centre for High Performance Computing and Communications.

[1] S. Trajmar and J. C. Nickel, Adv. At., Mol., Opt. Phys. **30**, 45 (1992).
[2] C. Lin Chun and L. W. Anderson, Adv. At., Mol., Opt. Phys. **29**, 1 (1992).
[3] T. Y. Jiang, Z. Shi, C. H. Ying, L. Vuskovic, and B. Bederson, Phys. Rev. A **51**, 3773 (1995).
[4] R. T. Sang, P. M. Farrell, D. H. Madison, W. R. MacGillivray, and M. C. Standage, J. Phys. B **27**, 1187 (1994).
[5] R. E. Scholten, S. R. Lorentz, J. McClelland, M. H. Kelly, and R. J. Celotta, J. Phys. B **24**, L653 (1991).
[6] H. W. Hermann and I. V. Hertel, Z. Phys. A **307**, 89 (1982).
[7] I. V. Hertel and W. Stoll, Adv. At. Mol. Phys. **13**, 1113 (1977).
[8] G. F. Hanne, J. J. McClelland, R. E. Scholten, and R. J. Celotta, J. Phys. B **26**, L753 (1993).
[9] Y. Li and P. W. Zetner, J. Phys. B **27**, L293 (1994).
[10] M. R. Law and P. J. O. Teubner, J. Phys. B **28**, 2257 (1995).
[11] Y. Li and P. W. Zetner, Phys. Rev. A **49**, 950 (1994).
[12] Y. Li and P. W. Zetner, J. Phys. B **28**, 5751 (1995).
[13] Y. Li and P. W. Zetner, J. Phys. B **29**, 1803 (1996).
[14] Y. Li and P. W. Zetner, J. Phys. B **25**, 3187 (1992).
[15] P. W. Zetner, Y. Li, and S. Trajmar, Phys. Rev. A **48**, 495 (1993).
[16] P. W. Zetner, S. Trajmar, S. Wang, I. Kanik, G. Csanak, R. E. H. Clark, J. Abdallah, Jr., and J. C. Nickel, J. Phys. B **30**, 5317 (1997).
[17] C. Moore, *Atomic Energy Levels as Derived from Analysis of Optical Spectra*, Natl. Bur. Stand. (U.S.), Circ. No. 467 (U.S. GPO, Washington, D.C., 1958).
[18] P. W. Zetner, S. Trajmar, S. Wang, I. Kanik, G. Csanak, R. E. H. Clark, J. Abdallah, Jr., and J. C. Nickel (unpublished).
[19] H. W. Hermann, thesis, Universität Kaiserslautern, Germany, 1979 (unpublished).
[20] N. Andersen, J. W. Gallagher, and I. V. Hertel, Phys. Rep. **165**, 1 (1988).
[21] I. Bray and A. T. Stelbovics, Phys. Rev. A **40**, 6995 (1992).
[22] V. Karaganov, I. Bray, and P. J. O. Teubner, J. Phys. B (to be published).
[23] I. Bray, Phys. Rev. A **49**, 1066 (1994).
[24] D. V. Fursa and I. Bray, Phys. Rev. A **52**, 1279 (1995).
[25] D. V. Fursa and I. Bray, J. Phys. B **30**, 5895 (1997).
[26] D. V. Fursa and I. Bray, Phys. Rev. A **57**, R3150 (1998).
[27] S. Trajmar, I. Kanik, M. A. Khakoo, L. LeClair, I. Bray, D. V. Fursa, and G. Csanak, J. Phys. B **31**, L393 (1998).
[28] D. F. Register, S. Trajmar, G. Csanak, S. W. Jensen, M. A. Fineman, and R. T. Poe, Phys. Rev. A **28**, 151 (1983).
[29] P. W. Zetner, S. Trajmar, and G. Csanak, Phys. Rev. A **41**, 5980 (1990).
[30] J. Macek and I. V. Hertel, J. Phys. B **7**, 2173 (1974).
[31] D. M. Brink and G. R. Satchler, *Angular Momentum* (Clarendon, Oxford, 1975).
[32] K. Blum, *Density Matrix Theory and Applications* (Plenum, New York, 1981).
[33] E. Hulpke, E. Paul, and W. Paul, Z. Phys. **177**, 257 (1964).
[34] A. F. Bernhardt, D. E. Duerre, J. R. Simpson, and L. L. Wood, J. Opt. Soc. Am. **66**, 416 (1976).
[35] C. Laughlin and G. A. Victor, in *Atomic Physics*, edited by S. J. Smith and G. K. Walters (Plenum, New York, 1972), Vol. 3, pp. 247–255.
[36] S. Hameed, A. Herzenberg, and M. G. James, J. Phys. B **1**, 822 (1968).
[37] E. Trefitz, J. Phys. B **7**, L342 (1974).
[38] C. W. Bauschlicher, Jr., R. L. Jaffe, S. R. Langhoff, F. G. Mascarello, and H. Partridge, J. Phys. D **18**, 2147 (1985).
[39] R. E. Clark, J. Abdallah, Jr., G. Csanak, and S. P. Kramer, Phys. Rev. A **40**, 2935 (1989).
[40] R. Srivastava, R. P. McEachran, and A. D. Stauffer, J. Phys. B **25**, 4033 (1992).
[41] V. Zeman, R. P. McEachran, and A. D. Stauffer, J. Phys. B **28**, 3063 (1995).
[42] S. Jensen, D. Register, and S. Trajmar, J. Phys. B **11**, 2367 (1978).
[43] S. Wang, S. Trajmar, and P. W. Zetner, J. Phys. B **27**, 1613 (1994).
[44] R. E. H. Clark and G. Csanak (private communication).
[45] A. Bizzarri and M. C. E. Huber, Phys. Rev. A **42**, 5422 (1990).
[46] C. D. Lin, R. Shingal, A. Jain, and W. Fritsch, Phys. Rev. A **39**, 4455 (1989).
[47] D. H. Madison, G. Csanak, and D. C. Cartwright, J. Phys. B **19**, 3361 (1986).

[48] M. Kohmoto and U. Fano, J. Phys. B **14**, L447 (1981).
[49] H. W. Hermann and I. V. Hertel, J. Phys. B **13**, 4285 (1980).
[50] P. W. Zetner, in *Proceedings of the XVIII International Conference on the Physics of Electronic and Atomic Collisions, Aarhus, Denmark, 1993,* edited by T. Andersen, B. Fastrup, F. Folkmannm, and H. Knudsen, AIP Conf. Proc. No. 295 (AIP Press, New York, 1993), p. 306.
[51] R. T. Brinkmann and S. Trajmar, J. Phys. E **14**, 245 (1981).
[52] K. E. Martus, S.-H. Zheng, and K. Becker, Phys. Rev. A **44**, 1682 (1991).